Mon. Not. R. Astron. Soc. **343,** 619–626 (2003)

Dynamical bar-mode instability of differentially rotating stars: effects of equations of state and velocity profiles

Masaru Shibata, Shigeyuki Karino★ and Yoshiharu Eriguchi

Department of Earth Science and Astronomy, Graduate School of Arts and Sciences, University of Tokyo, Komaba, Meguro, Tokyo 153-8902, Japan

Accepted 2003 April 8. Received 2003 April 3; in original form 2003 January 15

ABSTRACT

As an extension of our previous work, we investigate the dynamical instability against non-axisymmetric bar-mode deformations of differentially rotating stars in Newtonian gravity by varying the equations of state and velocity profiles. We performed the numerical simulation and the follow-up linear stability analysis by adopting polytropic equations of state with polytropic indices $n = 1$, $3/2$ and $5/2$, and with two types of angular velocity profiles (the so-called j-constant-like and Kepler-like laws). It is confirmed that rotating stars with a high degree of differential rotation are dynamically unstable against bar-mode deformation, even when the ratio of the kinetic energy to the gravitational potential energy β is of order 0.01. The criterion for the onset of bar-mode dynamical instability depends weakly on the polytropic index n and the angular velocity profile, as long as the degree of differential rotation is high. Gravitational waves from the final non-axisymmetric quasi-stationary states are calculated using the quadrupole formula. For proto-neutron stars of mass 1.4 $M_\odot$, radius $\sim$30 km and $\beta \lesssim 0.1$, such gravitational waves have a frequency of $\sim$600–1400 Hz, and the effective amplitude is larger than 10^{-22} at a distance of about 100 Mpc, irrespective of n and the angular velocity profile.

Key words: gravitational waves – stars: neutron – stars: oscillations – stars: rotation.

1 INTRODUCTION

In our previous paper (Shibata et al. 2002), we studied dynamical bar-mode stabilities of differentially rotating stars in Newtonian gravity. In that study, we adopted a polytropic equation of state with polytropic index $n = 1$ and the so-called 'j-constant-like' angular velocity profile in which the magnitude of the angular velocity decreases as ϖ^{-2} at large values of ϖ, where ϖ denotes the cylindrical radius. We found that rotating stars with a high degree of differential rotation are dynamically unstable even for $\beta \equiv |T/W| \sim 0.03$, where T and W are the rotational and gravitational potential energies. This value is much smaller than the long-believed criterion of $\beta \approx 0.27$ for the onset of the bar-mode dynamical instability of rotating stars (see Shibata et al. 2002 for a review). We also found that after the instability sets in, such unstable rotating stars with $0.03 \lesssim \beta \lesssim 0.15$ eventually settle down to non-axisymmetric ellipsoidal quasi-stationary states.

There are, however, two questions which have not been answered in the previous work (Shibata et al. 2002). One is associated with our choice of the j-constant-like angular velocity profile. It is well known that accretion discs around a central body with constant specific angular momentum are unstable against the Papaloizou–Pringle instability (Papaloizou & Pringle 1984). On the other hand, accretion discs are stable if the velocity profile is Kepler-like. One could claim that the bar-mode instability that we found would not be universal and might set in only for a very special rotational profile such as the j-constant-like law as in the Papaloizou–Pringle instability. In addition, we focused only on a stiff equation of state with $n = 1$ in the previous paper, so that one could also ask if the instability sets in for softer equations of state.

To answer these questions, we have performed numerical simulations of differentially rotating stars for which we vary the polytropic index and the angular velocity profile. We report the numerical results in this paper. We will show that irrespective of the polytropic index n and the angular velocity profile, a rotating star with a high degree of differential rotation is dynamically unstable against bar-mode deformation even when β is of order 0.01. We will also show that an unstable star with a small value of β eventually settles down to a non-axisymmetric quasi-stationary state, which is a strong emitter of quasi-periodic gravitational waves.

The paper is organized as follows. In Section 2, we describe our methods of numerical analysis, and the numerical results are presented in Section 3. Section 4 is devoted to a summary and discussion. Throughout this paper, we use the geometrical units $G = c = 1$ where G and c denote the gravitational constant and the velocity of light, respectively.

★E-mail: karino@provence.c.u-tokyo.ac.jp

2 METHOD

2.1 Differentially rotating axisymmetric stars

We set a differentially rotating star in equilibrium, and investigate the dynamical stability. Rotating stars in equilibrium are modelled, using the polytropic equations of state, as $P = K\rho^{\Gamma}$ where P, ρ, K and $\Gamma = 1 + 1/n$ denote the pressure, density, polytropic constant and adiabatic index, respectively. We choose $n = 1$, $3/2$ and $5/2$ ($\Gamma = 2$, $5/3$ and $7/5$).

As the angular velocity profile $\Omega(\varpi)$, we choose the so-called j-constant-like law

$$\Omega = \frac{\Omega_0 A^2}{\varpi^2 + A^2}, \tag{1}$$

and the so-called Kepler-like law

$$\Omega = \Omega_0 \left(\frac{A^2}{\varpi^2 + A^2}\right)^{3/4}, \tag{2}$$

where A is a constant, and Ω_0 is the angular velocity about the symmetric axis. The parameter A controls the steepness of the angular velocity profile: for smaller values of A, the profile is steeper and as $A \to \infty$, the rigid rotation is recovered. In this work, the values of A are chosen to satisfy $0.1 \leqslant \hat{A} \equiv A/R_{\rm eq} \leqslant 1$, where $R_{\rm eq}$ is the equatorial radius of the rotating star. For the rotation laws (1) and (2), at large cylindrical radius, Ω behaves asymptotically as ϖ^{-2} and $\varpi^{-3/2}$. This is why we refer to the profiles (1) and (2) as the j-constant-like and Kepler-like laws.

In the limit as $A \to 0$ with the profile (1), the specific angular momentum becomes constant everywhere and Ω diverges at $\varpi = 0$. We note that this profile has often been used in studies of non-axisymmetric instabilities in tori and annuli (Papaloizou & Pringle 1984; Goodman & Narayan 1988; Tohline & Hachisu 1990; Andalib, Tohline & Christodoulou 1997). Here, however, we do not consider tori and annuli and focus only on spheroidal stars for which the density is not zero at $\varpi = 0$. Thus, we cannot adopt this limiting profile.

A rotating star is determined in terms of $\beta = T/|W|$ and $\hat{A}$, for a given rotational profile and polytropic index. Thus, in the following we often refer to these two parameters to specify a rotating star. Here, T and W are defined as

$$T = \frac{1}{2}\int \rho\varpi^2\Omega^2 \, {\rm d}^3x, \tag{3}$$

$$W = \frac{1}{2}\int \rho\phi \, {\rm d}^3x, \tag{4}$$

where ρ and ϕ are the mass density and the Newtonian gravitational potential. To specify a particular model, we may choose the axis ratio of the rotating stars to be $C_{\rm a}$ instead of β. Here $C_{\rm a}$ is defined as the ratio of the polar radius $R_{\rm p}$ to the equatorial radius $R_{\rm eq}$, i.e. $C_{\rm a} = R_{\rm p}/R_{\rm eq}$. For the equations of state and the angular velocity profiles that we study here, the value of $C_{\rm a}$ monotonically decreases with an increase of β for a given set of $\hat{A}$ and n. This is the reason that $C_{\rm a}$ can be a substitute for β.

2.2 Investigation of dynamical stability

To investigate the dynamical stability against non-axisymmetric bar-mode deformations, we performed a numerical simulation as well as a linear stability analysis. We explain the methods of our numerical computation separately below.

2.2.1 Numerical simulation

In the hydrodynamic simulation, we initially superimpose a non-axisymmetric density perturbation on to an axisymmetric equilibrium star. We focus mainly on the fundamental bar mode, and simply add a nodeless density perturbation of the form

$$\delta\rho = \delta\rho_0(\varpi, z)\frac{x^2 - y^2}{R_{\rm eq}^2}, \tag{5}$$

where $\rho_0(\varpi, z)$ denotes the density of the axisymmetric configuration and δ is a constant. Throughout this work, we choose $\delta = 0.1$. For simplicity, the velocity is left unperturbed at $t = 0$. The growth of the bar mode can be followed by monitoring the distortion parameter

$$\eta \equiv \left(\eta_+^2 + \eta_\times^2\right)^{1/2}, \tag{6}$$

where

$$\eta_+ \equiv \frac{I_{xx} - I_{yy}}{I_{xx} + I_{yy}}, \tag{7}$$

$$\eta_\times \equiv \frac{2I_{xy}}{I_{xx} + I_{yy}}, \tag{8}$$

and $I_{ij}(i, j = x, y, z)$ denotes the quadrupole moment defined by

$$I_{ij} = \int \rho x^i x^j \, {\rm d}^3x, \tag{9}$$

where $x^i = (x, y, z)$. Simulations are performed using a 3D numerical hydrodynamic implementation in Newtonian gravity (Shibata et al. 1997; see also Shibata 2000 for results of various test simulations with the identical hydrodynamic numerical scheme but in general relativity). We adopt a fixed uniform grid of size $141 \times 141 \times 141$ in x, y, z coordinates, which covers an equatorial radius with 50 grid points initially. We also performed test simulations of size $71 \times 71 \times 71$ (i.e. the grid spacing becomes twice as large) for several selected cases and confirmed that the results depend weakly on the grid resolution. We assume reflection symmetry with respect to the equatorial plane. Since several of the rotating stars that we chose have a flattened configuration, we set the grid spacing of z to half of that of x and y.

2.2.2 Linear stability analysis

In the linear stability analysis, we employ the scheme developed by Karino et al. (2000) and Karino, Yoshida & Eriguchi (2001). The Euler perturbations of the physical quantities are replaced by functions of the form $f(r, \theta)\, {\rm e}^{{\rm i}m\varphi - {\rm i}\omega t}$ in the linearized hydrodynamic equations. Here m is the azimuthal mode number. As a result, the problem reduces to an eigenvalue problem for an eigenvalue ω and the corresponding eigenfunctions of the perturbed quantities. We assume an adiabatic relation between the Euler perturbation of the pressure and of the density. Since the fundamental mode of the $m = 2$ or bar-type oscillations is nodeless, we checked whether the obtained eigenfunctions satisfy that condition. We have analysed the stability of the equilibrium configurations of $n = 1$ polytropes for two rotation laws (1) and (2) with several values of $\hat{A}$.

3 NUMERICAL RESULTS

3.1 Dynamical bar-mode stability

3.1.1 Results of the numerical simulation

The dynamical stability is studied for various combination of Γ, $\hat{A}$ and β, and for two angular velocity profiles in the numerical simulation. In Figs 1 and 2, we summarize the results with regard to the dynamical bar-mode stability for the *j*-constant-like and Kepler-like angular velocity profiles, respectively. Here, the circles (crosses) indicate that the stars of a given set of $\hat{A}$ and β are dynamically unstable (stable). We focus only on spheroidal stars which are located below the dashed curves plotted in Figs 1 and 2. (If the value of β is larger than that on this curve for a given value of $\hat{A}$, the star is toroidal.)

It is found that many rotating stars with a high degree of differential rotation with $\hat{A} = 0.1$ and 0.3 are dynamically unstable even for β of order 0.01. In the case of the *j*-constant-like angular velocity profile, most rotating stars with $\beta \gtrsim 0.01$ and $\hat{A} = 0.3$ are dynamically unstable for both $\Gamma = 2$ and $5/3$. In the case of the Kepler-like angular velocity profile, the threshold of $\hat{A}$ for the onset of instability for a given set of β and Γ appears to be slightly smaller than that in the *j*-constant-like case. This is because the Kepler-like angular velocity profile is not as steep as the *j*-constant-like profile for the same value of $\hat{A}$. Indeed, for $\Gamma = 2$ and $5/3$ and for $\hat{A} = 0.3$, there is a wide parameter space around $\beta \sim 0.15$ in which the stars are stable against bar-mode deformation in the Kepler-like case. Such a wide parameter space is absent in the *j*-constant-like angular velocity profile for $\hat{A} = 0.3$. For $\hat{A} = 0.1$, however, stars in a wide range of β are unstable even in the Kepler-like angular velocity profile. Thus, *rotating stars with a high degree of differential rotation with β of order 0.01 are dynamically unstable even in the Kepler-like angular velocity profile.*

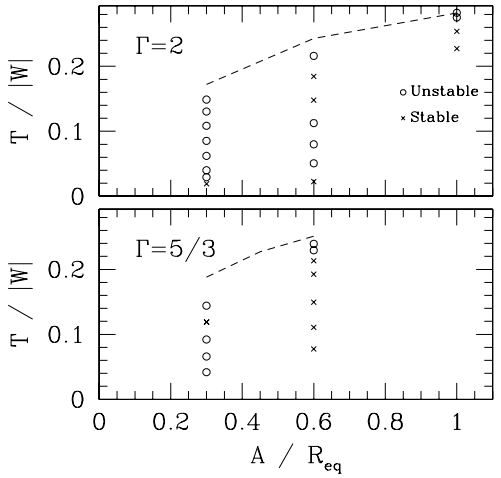

Figure 1. The dynamical bar-mode stability is shown in the β, $\hat{A}$ plane for the *j*-constant-like angular velocity profile. The circles and crosses indicate that the rotating stars are unstable and stable, respectively. The dashed curves denote the boundary which distinguishes spheroidal stars from toroidal stars (spheroidal stars are located below the curves).

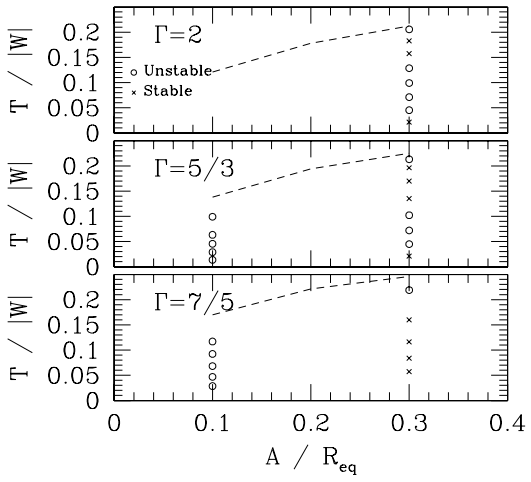

Figure 2. The same as Fig. 1 but for the Kepler-like angular velocity profile.

The threshold of $\hat{A}$ for the onset of dynamical instability for a given angular velocity profile also appears to depend on Γ: for a smaller value of Γ, the threshold of $\hat{A}$ is smaller. For example, compare the results with $\Gamma = 5/3$ and $7/5$ in Fig. 2. For $\Gamma = 5/3$, stars with $\hat{A} = 0.3$ and $0.03 \lesssim \beta \lesssim 0.1$ are unstable, but for $\Gamma = 7/5$, all the stars with $\beta < 0.2$ that we studied are stable for $\hat{A} = 0.3$. The reason is that rotating stars with smaller values of Γ have a more centrally condensed structure and as a result the effective degree of differential rotation of the central core for stars with soft equations of state can become very high only for a sufficiently small value of $\hat{A}$.

Rotating stars with a high degree of differential rotation are also dynamically unstable for high values of β ($\gtrsim$0.2) (see the results for $\hat{A} = 0.6$ and 1 for the *j*-constant-like law and for $\hat{A} = 0.3$ for the Kepler-like law). The axial ratio C_a of these stars is very small ($C_a \lesssim 0.3$). In particular, for unstable stars with the Kepler-like angular velocity profile with $\beta \gtrsim 0.2$ and $\hat{A} = 0.3$, $C_a \sim 0.15$. Thus, they have an almost toroidal shape. On the other hand, for unstable stars with a small value of β ($\lesssim$0.10), $C_a \gtrsim 0.5$ and hence the shape is not significantly toroidal.

An interesting feature is found for $\Gamma = 2$ and $\hat{A} = 0.6$ of the *j*-constant-like angular velocity profile, and for $\Gamma = 5/3$, 2 and $\hat{A} = 0.3$ of the Kepler-like angular velocity profile. In these cases, the stability does not change monotonically with increase of β:

(1) stars with a sufficiently small value of β ($\lesssim$0.01) are stable (we have not carried out simulations for $\beta < 0.01$, but since the value of C_a with $\beta \lesssim 0.01$ is larger than 0.9, i.e. the star is almost spherical, we assume that stars with $\beta \lesssim 0.01$ are stable);
(2) stars with $0.01 \lesssim \beta \lesssim 0.1$ are unstable;
(3) stars with $0.1 \lesssim \beta \lesssim 0.2$ are again stable; and
(4) stars with a sufficiently large value of β ($\gtrsim$0.2) are again unstable.

It has been widely believed that the value of β is a good indicator to distinguish between unstable and stable stars. The examples shown here, however, illustrate that β is not a good indicator for the determination of dynamical stability of rotating stars with a high degree of differential rotation.

The reason the stability does not change monotonically with β is not clear. The likely reason is that the mode associated with the stability for a high value of β is different from that for a small value. This interpretation cannot, however, be proved at present because of the following facts.

(i) The property of the unstable modes for a high value of β, such as the perturbed density profile and the magnitude itself ($\beta \gtrsim 0.2$), is essentially the same as that for the well-known bar mode (i.e. the $m = 2$ toroidal mode, see Chandrasekhar 1969). Hence, we identify the unstable modes with a high value of β with the *f* modes.

(ii) On the other hand, for a small value of β, the perturbed density profile is also nodeless, and furthermore the real part of the eigenfrequency is approximately proportional to $(M/R_{\rm eq}^3)^{1/2}$ (see Figs 10 and 11 below). These are the properties that the f mode should have. This suggests that the unstable modes for a small value of β might also be f modes.

We suspect that there is something different between two unstable modes of high and low values of β. To find the difference, however, it is necessary to understand precisely the definition of the f mode against the bar deformation for *differentially rotating stars*. It is not clear at present what properties, besides the nodeless density profile and the eigenfrequency of order of magnitude $\sim(M/R_{\rm eq}^3)^{1/2}$, characterize the f mode, i.e. we do not know what to prove. Precisely defining the f mode for differentially rotating stars is beyond scope of this paper, and is left as a problem for the future.

Before closing this section, we address the following point. As pointed out by Centrella et al. (2001), dynamical instability for the $m = 1$ mode may set in for rotating stars with a high degree of differential rotation. We have found no evidence that such instability sets in. This seems to be due to the fact that we adopted only the stiff equations of state. Centrella et al. (2001) studied the instability for differentially rotating stars with a very soft equation of state with $n = 10/3$. In such a soft equation of state, the instability associated with the $m = 1$ mode plays an important role. However, this is not likely to be the case in the stiff equations of state. Indeed, recently Saijo et al. (2003) have pointed out that the instability of the $m = 1$ mode sets in only for differentially rotating stars with very soft equations of state ($n \gtrsim 2.5$) and with a large value of β ($\gtrsim 0.15$).

3.1.2 Results of the linear analysis

In Fig. 3, we display the numerical results of the linear stability analysis for the same equilibrium models as shown in Figs 1 and 2 for the $n = 1$ polytrope. These figures show that the results of the numerical simulation agree well with those of the linear stability analysis, which confirms the conclusion that rotating stars with a high degree of differential rotation are dynamically unstable even for small values of β, irrespective of the angular velocity profile. We note that the solid curve in the upper panel of Fig. 3 denotes the threshold of dynamical stability (i.e. above this curve the star is dynamically unstable) against the well-known bar mode (Chandrasekhar 1969) which was calculated and reported by Karino & Eriguchi (2003).

3.2 Fate of unstable stars

In this section, we focus on rotating stars with the Kepler-like angular velocity profile, since the results for the j-constant-like angular velocity profile with $\Gamma = 2$ are presented in the previous paper (Shibata et al. 2002) and, moreover, we have found that the results for $\Gamma = 5/3$ show qualitatively identical features.

In Figs 4–7, we display the time evolution of η as a function of $\Omega_0 t$ for $(\Gamma, \hat{A}) = (2, 0.3), (5/3, 0.3), (5/3, 0.1)$ and $(7/5, 0.1)$. As shown here, the value of η does not reach a value of order 1 but saturates at order 0.1. This implies that the growth of the instability saturates at a weakly non-linear stage. We note that for unstable stars with $\beta \gtrsim 0.2$ and $\hat{A} = 0.3$, the value of η increases to ~ 1 irrespective of Γ, implying that a highly deformed star is produced. There are several numerical simulations in which such a highly non-axisymmetric structure results after the onset of dynamical instability of differentially rotating stars with a high value of β (e.g. Williams & Tohline 1987, 1988; Houser & Centrella 1996). The outcome of simulations

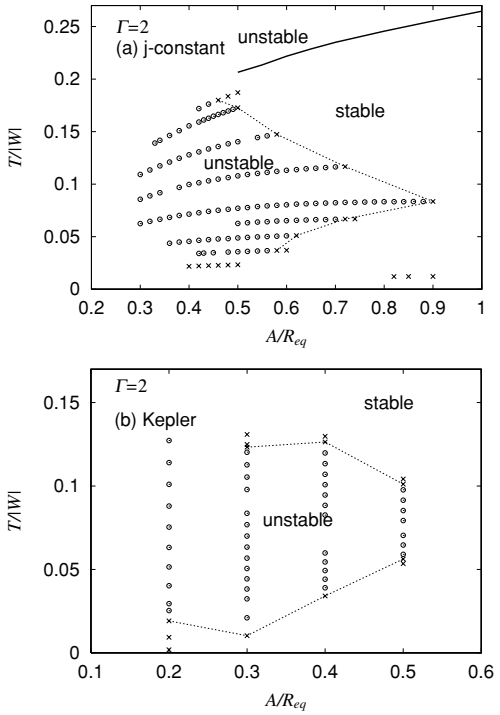

Figure 3. The results of the linear stability analysis are shown in the β, $\hat{A}$ plane for (a) the j-constant-like and (b) the Kepler-like angular velocity profiles. The circles and crosses indicate that the rotating stars are unstable and stable, respectively. The solid curve in the upper panel denotes the threshold of the dynamical instability against the well-known bar mode which was calculated by Karino & Eriguchi (2003). The dotted curves denote the approximate threshold of the stability for small values of β.

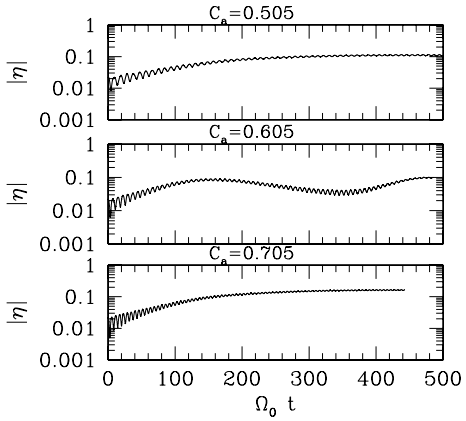

Figure 4. Time evolution of η as a function of $\Omega_0 t$ for $\Gamma = 2$ and $\hat{A} = 0.3$, and for the Kepler-like angular velocity profile.

for unstable stars with a high value of β found in the present numerical computation is qualitatively the same as that in previous papers. Thus, we do not discuss the results for such cases in the following.

After the perturbation saturates, the amplitude of η settles down to a value of order 0.1. The approximate final values of η are

$$\eta_{\rm f} \begin{cases} \sim 0.1 & \text{for} \quad (\Gamma, \hat{A}) = (2, 0.3), \\ \lesssim 0.1 & \text{for} \quad (\Gamma, \hat{A}) = (5/3, 0.3), \\ \sim 0.2 & \text{for} \quad (\Gamma, \hat{A}) = (5/3, 0.1), \\ \sim 0.03 & \text{for} \quad (\Gamma, \hat{A}) = (7/5, 0.1). \end{cases} \tag{10}$$

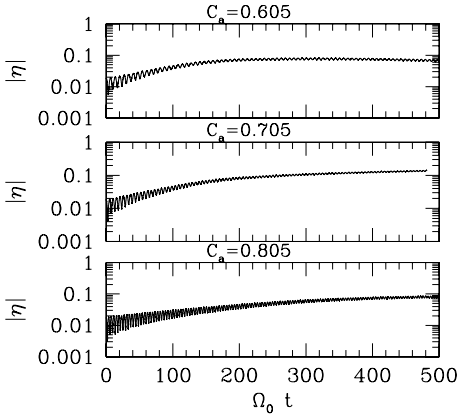

Figure 5. The same as Fig. 4 but for $\Gamma = 5/3$ and $\hat{A} = 0.3$.

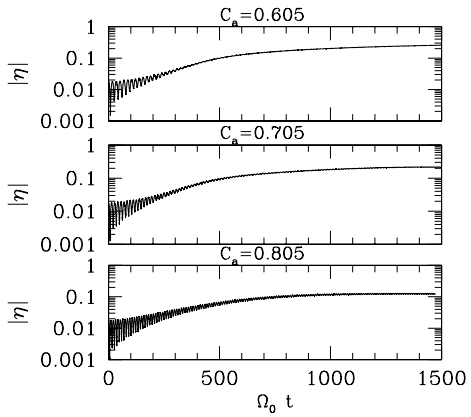

Figure 6. The same as Fig. 4 but for $\Gamma = 5/3$ and $\hat{A} = 0.1$.

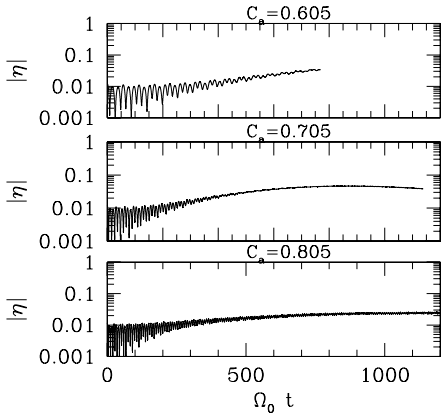

Figure 7. The same as Fig. 4 but for $\Gamma = 7/5$ and $\hat{A} = 0.1$.

Comparing the results of $(\Gamma, \hat{A}) = (5/3, 0.3)$ and $(5/3, 0.1)$ for an identical value of C_a, it is found that η_f is larger for the smaller value of $\hat{A}$. This implies that a stronger degree of differential rotation increases the magnitude of the non-axisymmetric deformation.

It is also found that for smaller values of Γ, the final value of η is smaller. This is because stars with smaller values of Γ have a more centrally condensed structure and hence the effective steepness of the differential rotation is smaller for smaller values of Γ for a given set of C_a and $\hat{A}$.

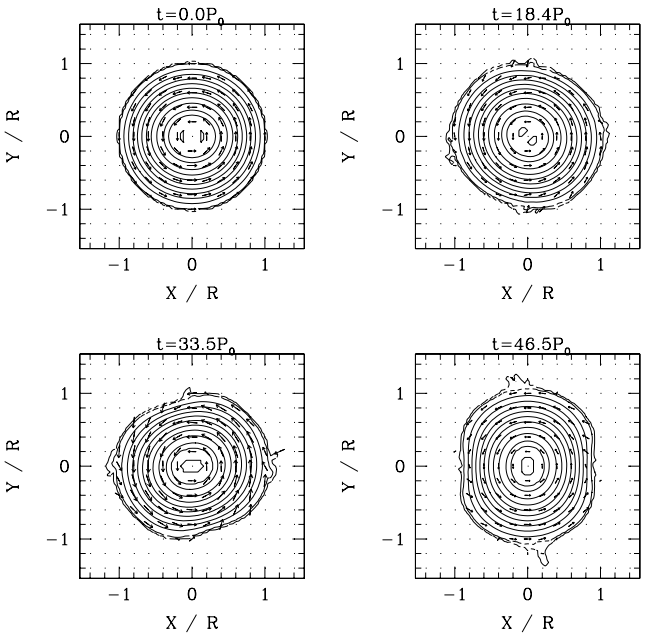

Figure 8. The density contour curves at selected time steps for $\Gamma = 2$, $\hat{A} = 0.3$ and $C_a = 0.7$ and for the Kepler-like angular velocity profile. Here, P_0 is $2\pi/\Omega_0$. The contour curves are drawn for $\rho/\rho_{max} = 0.95$, 0.9, 0.8, 0.7, 0.6, 0.5, 0.4, 0.3, 0.2, 0.1 0.01 and 0.001, where ρ_{max} denotes the maximum density at each time slice. The dashed curves are plotted for $\rho/\rho_{max} = 0.01$ and 0.001.

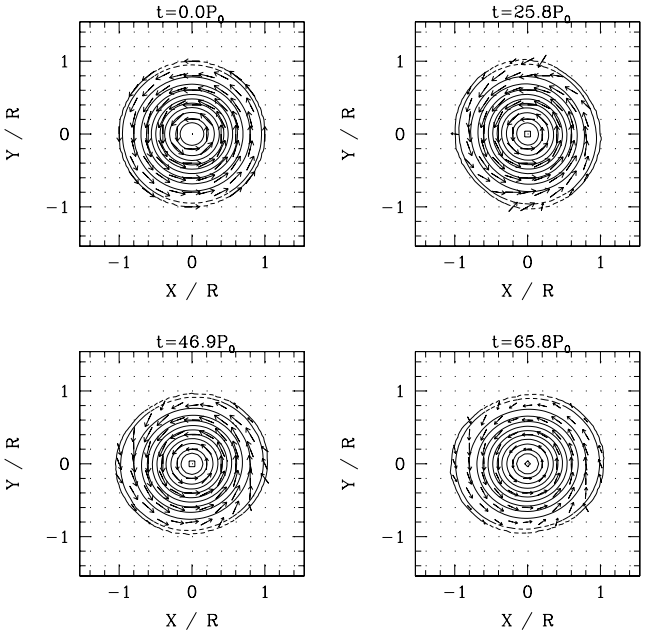

Figure 9. The same as Fig. 8, but for $\Gamma = 5/3$, $\hat{A} = 0.3$ and $C_a = 0.8$.

In Figs 8 and 9, we display the snapshots of the density contour curves in the equatorial plane at selected time steps for $(\Gamma, \hat{A}, C_a) = (2, 0.3, 0.7)$ and $(5/3, 0.3, 0.8)$. The value of β is about 0.071 and 0.045, respectively. In both cases, the initial non-axisymmetric perturbation grows, changing the shape of the rotating stars to ellipsoidal. However, the perturbation does not grow to the highly non-linear stage and hence neither a spiral arm nor a large bar is

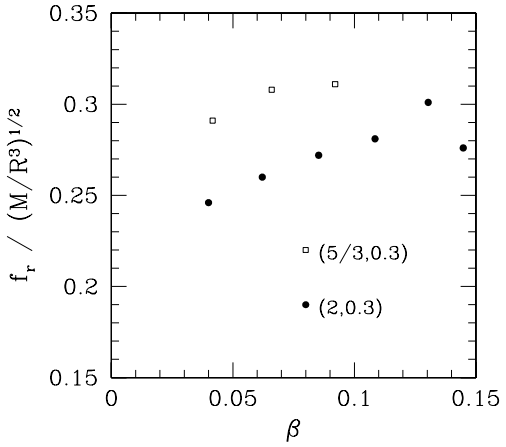

Figure 10. $\bar{f}_{\rm r}$ of the ellipsoids formed after the onset of dynamical instability for the *j*-constant-like angular velocity profile. Filled circles and open squares denote the results for $(\Gamma, \hat{A}) = (2, 0.3)$ and $(5/3, 0.3)$.

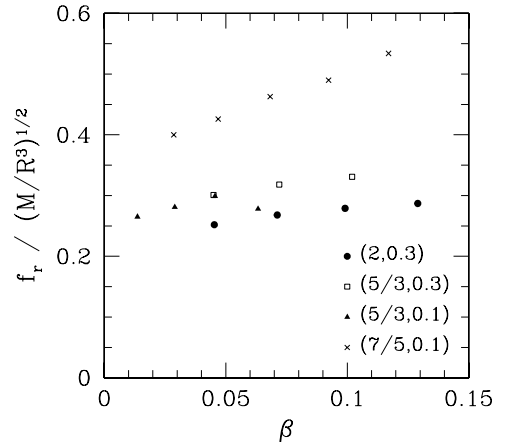

Figure 11. The same as Fig. 10, but for the Kepler-like angular velocity profile. Filled circles, open squares, filled triangles and crosses denote the results for $(\Gamma,\ \hat{A}) = (2,\ 0.3),\ (5/3,\ 0.3),\ (5/3,\ 0.1)$ and $(7/5, 0.1)$.

formed, in contrast to the outcome of simulations with a high value of $\beta \gtrsim 0.2$. Instead, a slightly deformed ellipsoid is the final outcome. Since the deformed ellipsoid is almost stationary, η_+ and $\eta_\times$ oscillate quasi-periodically in the late phase of the simulations. This result is qualitatively the same as that for stars with the *j*-constant-like angular velocity profile (Shibata et al. 2002).

In Figs 10 and 11, we show the frequency $f_{\rm r}$ of the oscillation of an ellipsoidal star in units of $(M/R_{\rm eq}^3)^{1/2}$ as a function of initial values of β for various sets of Γ and $\hat{A}$. The value of $f_{\rm r}$ is determined by the Fourier transform of η_+ in the time domain. We note that the rotational period of the ellipsoid is $2/f_{\rm r}$, and that the frequency of the gravitational waves is $f_{\rm r}$. It is interesting to note that for $\Gamma = 2$ and 5/3, the non-dimensional quantity $\bar{f}_{\rm r} \equiv f_{\rm r}(R_{\rm eq}^3/M)^{1/2}$ lies in a narrow range between 0.2 and 0.35, irrespective of $\hat{A}$, β and the angular velocity profile. For $\Gamma = 7/5$, $\bar{f}_{\rm r}$ is between 0.4 and 0.55, which is larger than the values for $\Gamma = 2$ and 5/3. However, it is still in a narrow range. The fact that the value of $\bar{f}_{\rm r}$ depends weakly on β suggests that the excited mode may be an *f* mode.

3.3 Gravitational waves

As discussed in our previous paper (Shibata et al. 2002), dynamically unstable rotating stars, which are deformed to non-axisymmetric ellipsoidal objects, are likely to be sources of quasi-periodic gravitational waves. In Figs 12–14, we show the gravitational waveforms of the + mode along the *z*-axis (h_+) and the luminosity ($\dot{E}$) as a

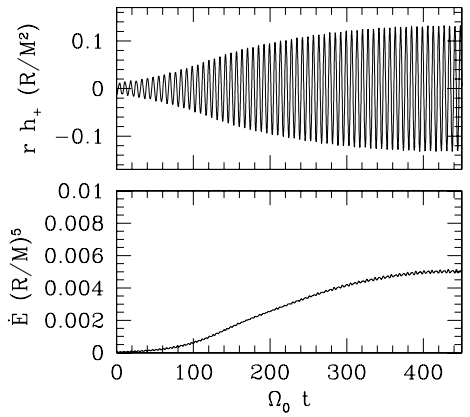

Figure 12. Gravitational waves for h_+ in units of $M^2/R_{\rm eq}$ and the luminosity of gravitational waves $\dot{E}$ in units of $(M/R_{\rm eq})^5$ as a function of $\Omega_0 t$ for $(\Gamma, \hat{A}) = (2, 0.3)$ and $C_{\rm a} = 0.705$ ($\beta \approx 0.071$).

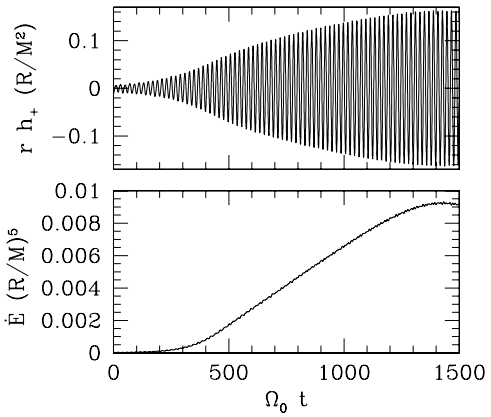

Figure 13. The same as Fig. 12, but for $(\Gamma, \hat{A}) = (5/3, 0.1)$ and $C_{\rm a} = 0.705$ ($\beta \approx 0.046$).

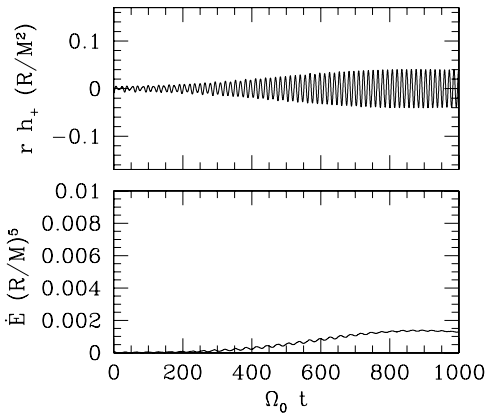

Figure 14. The same as Fig. 12, but for $(\Gamma, \hat{A}) = (7/5, 0.1)$ and $C_{\rm a} = 0.705$ ($\beta \approx 0.047$).

function of time for $(\Gamma, \hat{A}) = (2, 0.3)$, $(5/3, 0.1)$ and $(7/5, 0.1)$. For all the models discussed here, $C_a = 0.705$. The value of β is $\approx$0.071, 0.046 and 0.047, respectively. We note that the waveforms for the $\times$ mode are essentially the same as those for the + mode except for the phase difference of $\pi/4$. Here, we calculate gravitational waves using the quadrupole formula (Misner, Thorne & Wheeler 1973) and define the waveforms by

$$h_+ \equiv \frac{\ddot{I}_{xx} - \ddot{I}_{yy}}{r}, \quad h_\times \equiv \frac{2\ddot{I}_{xy}}{r}, \tag{11}$$

and the luminosity by

$$\dot{E} \equiv \frac{1}{5} \sum_{i,j} \mathcal{I}^{(3)}_{ij} \mathcal{I}^{(3)}_{ij}, \tag{12}$$

where

$$\mathcal{I}_{ij} = I_{ij} - \frac{\delta_{ij}}{3} \sum_k I_{kk},$$
$$\ddot{I}_{ij} = \frac{d^2 I_{ij}}{dt^2}, \quad \mathcal{I}^{(3)}_{ij} = \frac{d^3 \mathcal{I}_{ij}}{dt^3}, \tag{13}$$

and r is the distance from the source to the detector. h_+ and $h_\times$ are the waveforms observed along the z-axis.

In the early phase before the growth of the non-axisymmetric perturbation saturates, the amplitude of gravitational waves increases gradually, together with the magnitude of η. Then the growth of the amplitude saturates and subsequently quasi-periodic gravitational waves are emitted for a much longer time than the rotational period. The amplitude of quasi-periodic gravitational waves depends on Γ and $\hat{A}$, as in the case of the saturated value of η. For a given set of $\hat{A}$ and C_a (or β), it is smaller for smaller values of Γ, because a star with smaller values of Γ is more centrally condensed and hence the magnitudes of the quadrupole moments are smaller for identical mass and radius.

We found that for the parameters we studied ($\beta \lesssim 0.1$, $\hat{A} \leqslant 0.6$ and angular velocity profiles (1) and (2)), typical values of the amplitude and luminosity of gravitational waves for $\Gamma = 2$ are $rh_{+,\times} \sim 0.1$–$0.2(M^2/R_{eq})$ and $\dot{E} \sim 0.005$–$0.01\ (M/R_{eq})^5$. For $\Gamma = 5/3$, the magnitudes are only slightly smaller than those for $\Gamma = 2$. For $\Gamma = 7/5$, however, they are significantly smaller: $rh_{+,\times} \sim 0.05(M^2/R_{eq})$ and $\dot{E} \sim 0.001(M/R_{eq})^5$.

Using the results shown in Figs 12–14, we can estimate the expected effective amplitude of gravitational waves from the non-axisymmetric outcomes formed after the dynamical instability saturates. Here, we pay particular attention to proto-neutron stars which are likely to be formed soon after supernovae with mass $\sim$1.4 $M_\odot$ and with a radius of several tens of kilometres. For the luminosity $\dot{E} = 0.001\epsilon(M/R_{eq})^5$ where ϵ is a parameter of magnitude 1–10, the emission time-scale of gravitational waves can be estimated as

$$\tau \sim \frac{T}{\dot{E}} = 100\alpha_0\epsilon^{-1} \left(\frac{\beta}{0.1}\right) \left(\frac{R_{eq}}{M}\right)^4 M$$
$$= 6.1\,\mathrm{s}\,\alpha_0\epsilon^{-1} \left(\frac{\beta}{0.1}\right) \left(\frac{R_{eq}}{30\,\mathrm{km}}\right)^4 \left(\frac{M}{1.4\,M_\odot}\right)^{-3}, \tag{14}$$

where we set $T = \alpha_0\beta M^2/R_{eq}$, and α_0 is a constant which depends on the value of Γ but very weakly on $\hat{A}$; for $\beta \lesssim 0.1$, $\alpha_0 \sim 0.8$, 0.9 and 1.2, for $\Gamma = 2$, 5/3 and 7/5, respectively, within $\sim$10 per cent error.

The characteristic frequency of gravitational waves is

$$f = f_r \approx 790\,\mathrm{Hz} \left(\frac{\bar{f}_r}{0.3}\right) \left(\frac{R_{eq}}{30\,\mathrm{km}}\right)^{-3/2} \left(\frac{M}{1.4\,M_\odot}\right)^{1/2}. \tag{15}$$

Assuming that the non-axisymmetric perturbation would not be dissipated by viscosity or magnetic fields on the emission time-scale of gravitational waves (e.g. Baumgarte, Shapiro & Shibata 2000), the accumulated cycles of a gravitational wave-train N are estimated as

$$N \equiv f\tau = 4.8 \times 10^3 \alpha_0 \left(\frac{\epsilon}{5}\right)^{-1} \left(\frac{\bar{f}_r}{0.3}\right)$$
$$\times \left(\frac{\beta}{0.1}\right) \left(\frac{R_{eq}}{30\,\mathrm{km}}\right)^{5/2} \left(\frac{M}{1.4\,M_\odot}\right)^{-5/2}. \tag{16}$$

The effective amplitude of gravitational waves is defined by $h_{eff} \equiv N^{1/2}h$ where h denotes the characteristic amplitude of periodic gravitational waves. Using this relation, we find (Thorne 1987; Lai & Shapiro 1995; Liu & Lindblom 2001; Liu 2002)

$$h_{eff} \approx 3.2 \times 10^{-22} \alpha_0^{1/2} \left(\frac{\bar{h}}{0.1}\right) \left(\frac{\epsilon}{5}\right)^{-1/2} \left(\frac{\beta}{0.1}\right)^{1/2} \left(\frac{\bar{f}_r}{0.3}\right)^{1/2}$$
$$\times \left(\frac{R_{eq}}{30\,\mathrm{km}}\right)^{1/4} \left(\frac{M}{1.4\,M_\odot}\right)^{3/4} \left(\frac{100\,\mathrm{Mpc}}{r}\right) \tag{17}$$

where $\bar{h} \equiv hrR_{eq}/M^2$. Since $\bar{f}_r$, $\bar{h}$, ϵ and β depend on the values of Γ, $\hat{A}$ and C_a, h_{eff} can vary by a factor of $\sim$3. However, for all the rotating stars that we studied, h_{eff} is always larger than 10^{-22} at a distance of $\sim$100 Mpc with $R_{eq} \sim$30 km and $M \sim 1.4\,M_\odot$. Furthermore, the frequency of gravitational waves is about 1 kHz for $R_{eq} \sim$ 30 km and $M \approx 1.4\,M_\odot$. Thus, gravitational waves from proto-neutron stars with a high degree of differential rotation, of mass $\sim$1.4 $M_\odot$ and with radius $\gtrsim$ 30 km at a distance of $\sim$100 Mpc, are likely to be sources for laser interferometric detectors such as LIGO (Thorne 1995), if the other dissipation processes are negligible.

4 SUMMARY AND DISCUSSION

We have studied the dynamical bar-mode instability of differentially rotating stars of polytropic equations of state. We chose three polytropic indices and two angular velocity profiles in this study. We found that rotating stars with a high degree of differential rotation are dynamically unstable against non-axisymmetric bar-mode deformation even with $\beta \ll 0.27$, irrespective of the polytropic indices and angular velocity profile. The criterion of the value of β for the onset of the instability depends on the rotational profile and the equations of state, but the dependence is very weak if the degree of differential rotation is high enough so that $\hat{A} \sim 0.1$.

We estimated the effective amplitude of gravitational waves from non-axisymmetric objects formed after the onset of dynamical instability. For typical proto-neutron stars of mass $\sim$1.4 $M_\odot$ and radius several tens of kilometres, the effective amplitude of gravitational waves at a distance of $\sim$100 Mpc is larger than 10^{-22}, and the frequency is $\sim$ 1 kHz. Therefore, gravitational waves can be sources for laser interferometric detectors such as advanced LIGO (e.g. Thorne 1995).

As we mentioned above, this conclusion is drawn under the assumption that dissipation of non-axisymmetric perturbations by viscosity and magnetic fields is negligible. The dissipation time-scale due to molecular viscosity and magnetic braking is likely to be longer than 10 s (e.g. Baumgarte et al. 2000). Thus, these effects can be safely neglected. However, turbulent magnetic viscosity (Balbus & Hawley 1998) may be relevant for redistribution of the angular momentum profile. This implies that a differentially rotating star might be forced to adopt a rigidly rotating state on a dynamical time-scale and hence the non-axisymmetric structure might disappear. Much theoretical work has shown that the magnetic viscous

effect can redistribute the angular momentum distribution of accretion discs around central objects on a dynamical time-scale (Balbus & Hawley 1998). To the best of our knowledge, however, there is no work on the magnetic field effect for self-gravitating rotating stars. The magnetic field would redistribute the angular momentum of the differentially rotating stars on a dynamical time-scale, but it is not clear whether it is strong enough to force rotating stars into an axisymmetric state in a dynamical time-scale. To clarify this problem, it is necessary to carry out magnetohydrodynamic simulations for rotating stars. Such work should be done in the future.

ACKNOWLEDGMENTS

We thank L. Lindblom and I. Hachisu for discussion and comments. Numerical simulations were performed on FACOM VPP5000 in the data processing center of the National Astronomical Observatory of Japan. This work was in part supported by a Japanese Monbu-Kagaku-Sho Grant (Nos. 12640255, 13740143 and 14047207). SK is supported by a JSPS Research Fellowship for Young Scientists.

REFERENCES

Andalib S. W., Tohline J. E., Christodoulou D. M., 1997, ApJS, 108, 471
Balbus S. A., Hawley J. F., 1998, Rev. Mod. Phys., 70, 1
Baumgarte T. W., Shapiro S. L., Shibata M., 2000, ApJ, 528, L29
Centrella J. M., New K. C. B., Lowe L., Brown J. D., 2001, ApJ, 550, L193
Chandrasekhar S., 1969, Ellipsoidal Figures of Equilibrium. Yale Univ. Press, New Haven
Goodman J., Narayan R., 1988, MNRAS, 231, 97
Houser J. L., Centrella J. M., 1996, Phys. Rev. D, 54, 7278
Karino S., Eriguchi Y., 2003, ApJ, submitted
Karino S., Yoshida S'i., Yoshida S'j., Eriguchi Y., 2000, Phys. Rev. D, 62, 084012
Karino S., Yoshida S'i., Eriguchi Y., 2001, Phys. Rev. D, 64, 024003
Lai D., Shapiro S. L., 1995, ApJ, 442, 259
Liu Y. T., 2002, Phys. Rev. D, 65, 124003
Liu Y. T., Lindblom L., 2001, MNRAS, 342, 1063
Misner C. W., Thorne K. S., Wheeler J. A., 1973, Gravitation. W. H. Freeman and Company, New York
Papaloizou J. C. B., Pringle J. E., 1984, MNRAS, 208, 721
Saijo M., Baumgarte T. W., Shapiro S. L., 2003, (astro-ph/0302436)
Shibata M., 2000, Phys. Rev. D, 60, 104052
Shibata M., Oohara K., Nakamura T., 1997, Prog. Theor. Phys., 98, 1081
Shibata M., Karino S., Eriguchi Y., 2002, MNRAS, 334, L27
Thorne K. S., 1987, in Hawking S., Israel W., eds, 300 Years of Gravitation. Cambridge Univ. Press, Cambridge, p. 330
Thorne K. S., 1995, in Kolb E. W., Peccei R., eds, Proceeding of Snowmass 95 Summer Study on Particle and Nuclear Astrophysics and Cosmology. World Scientific, Singapore, p. 398
Tohline J. E., Hachisu I., 1990, ApJ, 361, 394
Williams H. A., Tohline J. E., 1987, ApJ, 315, 594
Williams H. A., Tohline J. E., 1988, ApJ, 334, 449

This paper has been typeset from a TEX/LATEX file prepared by the author.